# Supplementary Information on Phase Equilibrium during Synthesis of $LiNi_{0.46}Mn_{1.54}O_4$: Comprehensive X-ray & Neutron Powder Diffraction Study

Ilia Tertov [1,2,3], François Fauth [4], Emmanuelle Suard [1], Thomas Hansen [1], François Weill [2], Pierre-Etienne Cabelguen [5], Christian Masquelier [3,6,7,*], Laurence Croguennec [2,6*].

[1] Institut Laue-Langevin, 38042, Grenoble, France

[2] Univ. Bordeaux, CNRS, Bordeaux INP, ICMCB UMR 5026, F-33600, Pessac, France

[3] Laboratoire de Réactivité et de Chimie des Solides, Université de Picardie Jules Verne, CNRS-UMR 7314, F-80039, Amiens Cedex 1, France

[4] CELLS-ALBA Synchrotron, Cerdanyola del Vallès, E-08290 Barcelona, Spain

[5] Umicore, 31 rue du marais, Brussels BE-1000, Belgium

[6] RS2E, Réseau sur le stockage électrochimique de l'énergie, FR CNRS 3459, F-80039, Amiens Cedex 1, France

[7] Institut Universitaire de France, 103 boulevard Saint-Michel, 75005 Paris, France

Corresponding authors:

laurence.croguennec@icmcb.cnrs.fr (L. Croguennec);

christian.masquelier@u-picardie.fr (C. Masquelier)

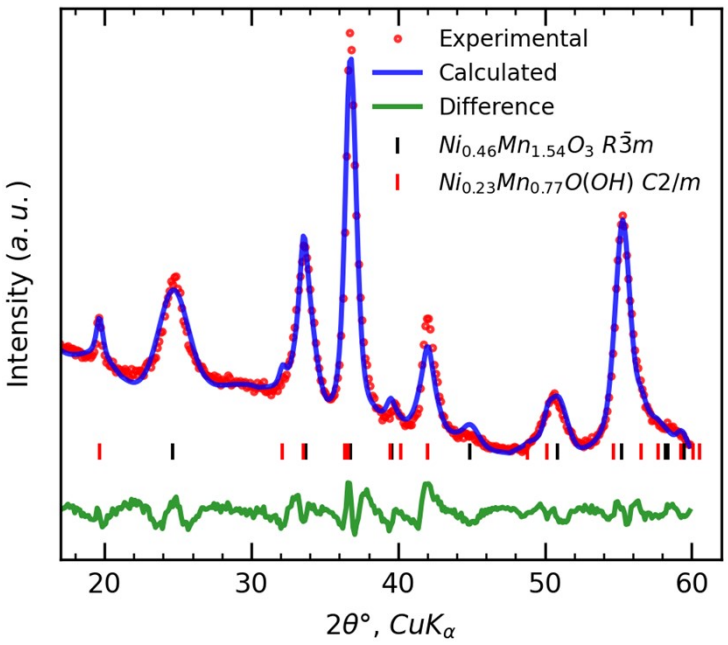


**Figure S1**. Experimental points, calculated and difference plots with corresponding Bragg positions obtained after the Rietveld refinement of laboratory XRPD pattern of the sample, prepared by the firing of $Ni_{0.23}Mn_{0.77}(OH)_2$ at T = 400°C for 12 hours.

Dehydration of $Ni_{0.23}Mn_{0.77}(OH)_2$ at T ≈ 300°C results in formation of the new phase. Due to the presence of $Li_2CO_3$ in the mixture and the poor crystallinity of this new phase, identification of its crystal structure was not possible.

To identify this new phase, firing of $Ni_{0.23}Mn_{0.77}(OH)_2$ was carried out at 400°C for 12 hours under air. Phase analysis of the laboratory X-ray powder diffraction (XRPD) pattern of the resulting powder shows the formation of ilmenite-type $Ni_xMn_{2-x}O_3$ oxide as a main phase and $Ni_yMn_{1-y}O(OH)$ oxide-hydroxide as an impurity phase. For the Rietveld refinement, the structural models of $NiMnO_3$ (ICSD # 31853) and β-MnO(OH) (ICSD # 128280) were used with all structural parameters fixed for both phases except lattice parameters. Refinement of the chemical composition of both phases was challenging because of their poor crystallinity and similar scattering power of Mn and Ni atoms, so the chemical compositions were fixed to $Ni_{0.46}Mn_{1.54}O_3$ and $Ni_{0.23}Mn_{0.77}O(OH)$. Experimental points, calculated and difference profiles after the Rietveld refinement can be found in **Figure S2**. It should be noted that real chemical compositions can be different as the presence of structurally different phases may cause segregation of Mn and Ni cations, thus the following chemical composition $Ni_xMn_{2-x}O_3$ for the ilmenite-type phase and $Ni_yMn_{1-y}O(OH)$ for the oxide-hydroxide phase are more correct.

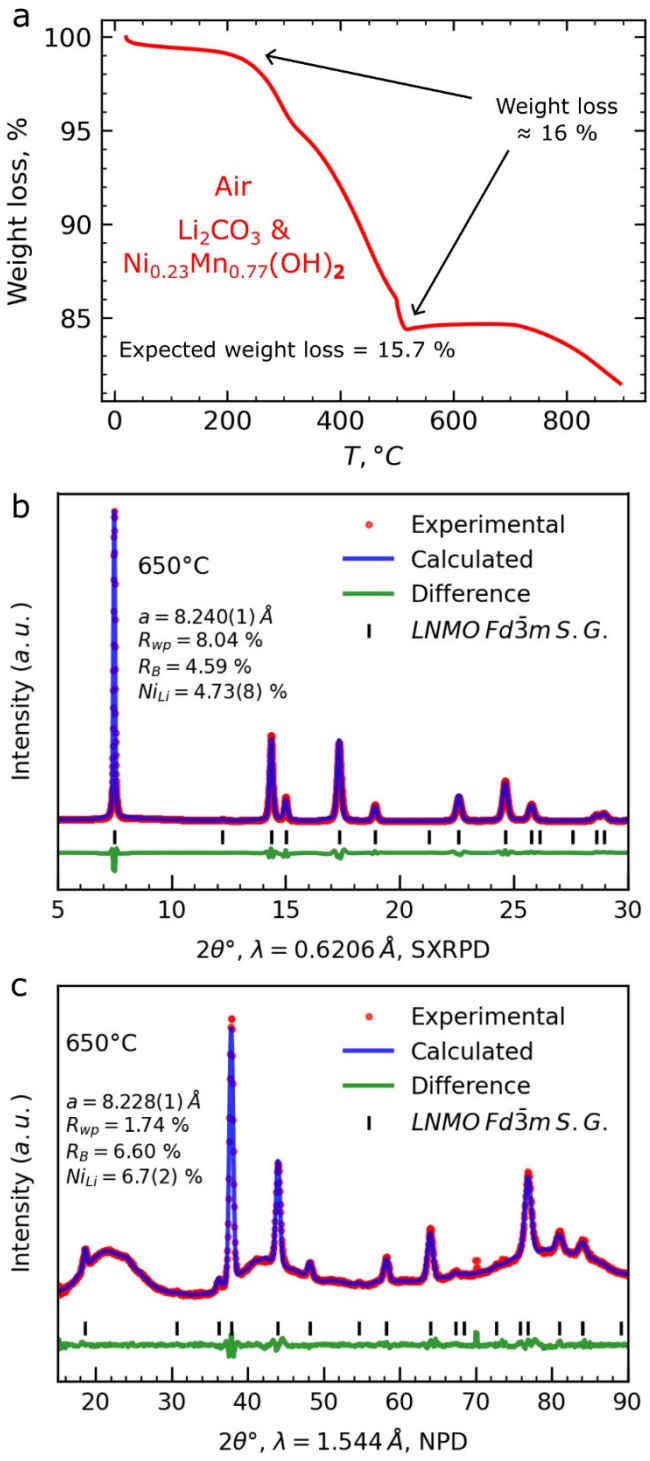


**Figure S2**. TG data for the mixture of $Li_2CO_3$ and $Ni_{0.23}Mn_{0.77}(OH)_2$ (5°C/min → 500°C, 1°C/min → 900°C) (a). Experimental points, calculated and difference plots after the Rietveld refinement of the SXRPD (b) and NPD (c) patterns at 650°C during in situ experiments

## Rietveld Refinement procedure

### *In situ* SXRPD

For the LNMO spinel phase, the structural model of disordered LNMO was used (ICSD # 180032). Coordinates of the O atom at the 32*e* sites and atomic displacement parameter (ADP) were refined. The occupancy factors of Mn and Ni at the 16*d* (octahedral) sites were fixed such as Mn/Ni = 77/23. As the difference Fourier analysis revealed an excess of the electronic density at the 8*a* (tetrahedral) sites, the Ni atoms were placed at the 8*a* sites and refined with the constraint: Li+Ni = 100%. The common ADP for the 8*a* and the 16*d* sites was refined. The structural model can be described by the following chemical formula: $(Li_{1-x}Ni_x)_{8a}(Ni_{0.46}Mn_{1.54})_{16d}O_4$.

For the different types of the impurity phases, different structural models were used. In the case of the Layered oxide impurity, the structural model of $LiNiO_2$ (ICSD # 78687) was used as an initial model. If resolution and statistics of the SXRPD patterns were sufficient (indicated in the main text), both Li and Ni atoms were placed at the 3*a* and the 3*b* sites and refined with the following constraint for each site: Li+Ni = 100%. Otherwise, the fixed chemical composition of $LiNiO_2$ was used. The ADP of the atoms at the 3*a* and 3*b* sites was equated to the common ADP for the 8*a* and the 16*d* sites in the LNMO spinel phase. The ADP of the oxygen atom at the 6*b* sites was equated to the ADP of the oxygen atom at the 32*e* sites in the LNMO spinel phase.

For the rock salt impurity, the structural model of $Li_{0.2}Ni_{0.8}O$ (ICSD # 71422) was used. If resolution and statistics of the SXRPD patterns were sufficient (indicated in the main text), the occupancy factor of Ni and Li at the 4*a* sites was refined with the following constraint: Li+Ni = 100%. Otherwise, the fixed chemical composition $Li_{0.2}Ni_{0.8}O$ was used. The ADP of the atoms at the 4*a* sites was equated to the common ADP for the 8*a* and the 16*d* sites in the LNMO spinel phase. The ADP of the oxygen atom at the 4*b* sites was equated to the ADP of the oxygen atom at the 32*e* sites in the LNMO spinel phase.

### *In situ* NPD

For the LNMO spinel phase, the structural model of disordered LNMO was used (ICSD # 180032). Coordinates of the oxygen atom at the 32*e* sites and atomic displacement parameter (ADP) were refined. The occupancy factors of Mn and Ni at

the 16*d* sites were refined with the following constraint: Ni+Mn = 100%. As in the case of *in situ* SXRPD, the Ni atoms were placed at the 8*a* sites to describe an increased atomic density. The occupancy factors of Ni and Li at the 8*a* sites were refined with the constraint: Li+Ni = 100%. The common ADP for the 8*a* and the 16*d* sites was refined. The structural model can be described by the following chemical formula: $(Li_{1-x}Ni_x)_{8a}(Ni_{0.5-y}Mn_{1.5+y})_{16d}O_4$.

For the Layered oxide impurity, the structural model of $LiNi_{0.5}Mn_{0.5}O_2$ (ICSD # 97790) was used. Due to low resolution, the fixed chemical composition of $LiNi_{0.5}Mn_{0.5}O_2$ was used.

Combined Rietveld refinement of the samples quenched from T = 600-700°C

For the combined Rietveld refinement of SXRPD and NPD patterns of the q600°C, q650°C and q700°C samples, the same structural model $(Li_{1-x}Ni_x)_{8a}(Ni_{0.5-y}Mn_{1.5+y})_{16d}O_4$, described above in the '*In situ* NPD' section was used.

For the q650°C 2h sample, the structural model of ordered LNMO was used (ICSD # 47491). Coordinates of the O atoms at the 8*c* and 24*e* sites and the common ADP for both sites were refined. Both Mn and Ni atoms were placed at the 4*b* sites (Ni sites) and the 12*d* sites (Mn sites). The occupancy factors of Ni and Mn were refined with the constraint Ni+Mn = 100% for each site. Ni atoms were placed at the 8*c* sites (Li sites) and refined with the constrain Li+Ni = 100%. The structural model can be described by the formula: $(Li_{1-x}Ni_x)_{8c}(Ni_{0.5-y}Mn_y)_{4b}(Mn_{1.5+z}Ni_z)_{12d}O_4$. Coordinates of Li and Ni atoms at the 8*c* sites and the ADP were refined. Coordinates of Ni and Mn atoms at the 12*d* sites were refined. The common ADP for the 4*b* and the 12*d* sites was refined.

To account for the broadening of the superstructure, an additional Lorentzian broadening of the superstructure reflections was refined with FullProf using size model #12.

Rietveld refinement of the SXRPD and NPD patterns of the samples quenched from T = 750-900°C

First, the Rietveld refinement of SXRPD patterns were carried out. The same structural models for all the phases were used as for the Rietveld refinement of *in situ* SXRPD

data. The chemical composition of layered oxide and rock salt phases were fixed to $LiNiO_2$ and $Li_{0.2}Ni_{0.8}O$ respectively.

Then, for the Rietveld refinement of NPD patterns, the structural model of the LNMO phase was expanded to $(Li_cNi_{1-y-c}Mn_y)_{8a}(Ni_{0.5-z}Mn_{1.5+z})_{16d}O_4$, where c represents the Li content at the 8*a* sites, derived from refinement of SXRPD data. In other words, the Li content at the 8*a* was obtained from the SXRPD data and fixed in the Rietveld refinement of NPD data, then the y parameter was refined. The occupancy factor z of Mn and Ni at the 16*d* sites were refined with the following constraint: Ni+Mn = 100%.

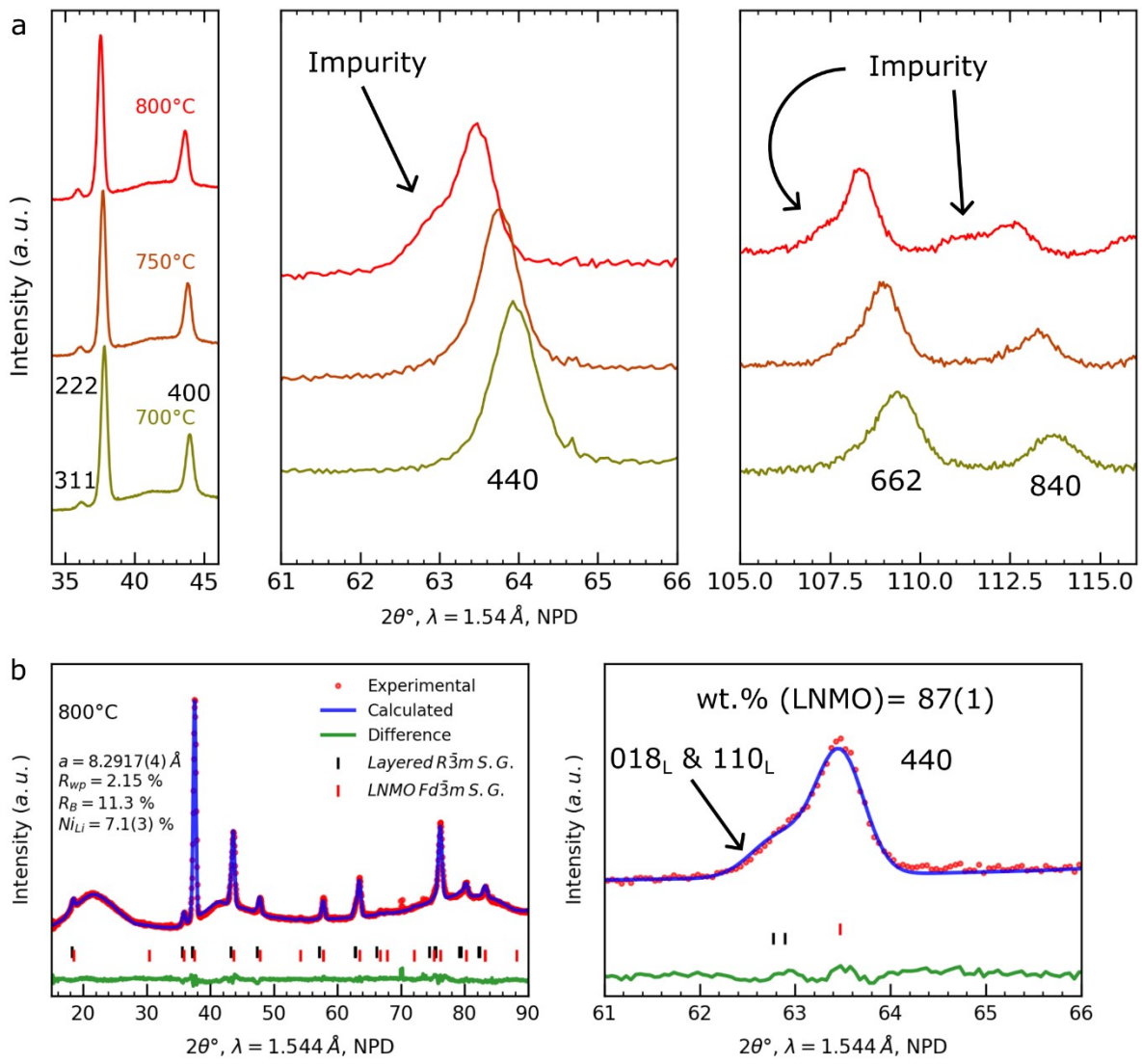


**Figure S3**. Selected 2θ ranges of in situ NPD patterns of the mixture of $Li_2CO_3$ and $Ni_{0.23}Mn_{0.77}(OH)_2$ at given temperatures (a). Experimental points, calculated and difference plots after the Rietveld refinement of the NPD pattern collected at 800°C (b).

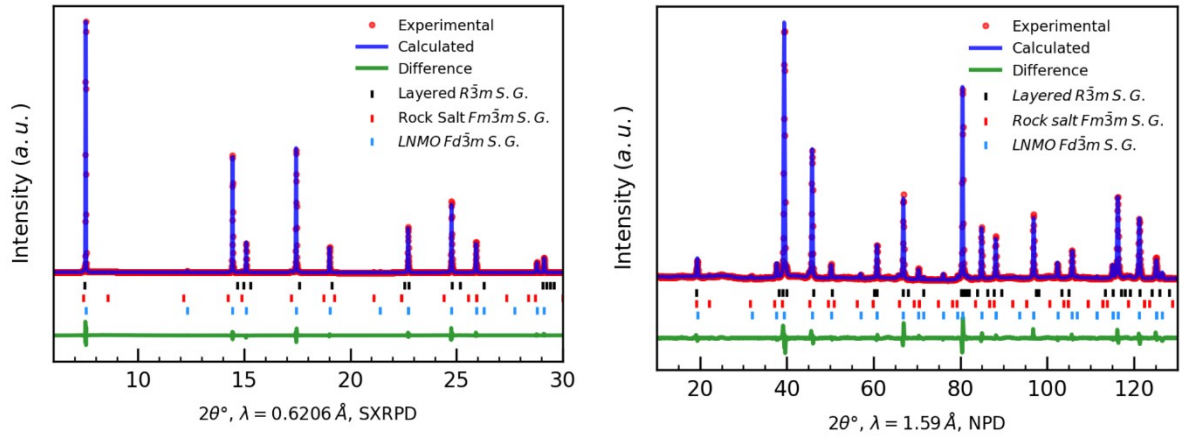


**Figure S4**. Experimental points, calculated and difference profiles obtained after the Rietveld refinement of the SXRPD pattern (left) and the NPD pattern (right) of the pristine LNMO sample $LiNi_{0.46}Mn_{1.54}O_4$.

**Combined Rietveld refinement of SXRPD and NPD data of the pristine sample**

For the LNMO spinel phase, the structural model of disordered LNMO was used (ICSD # 180032). Coordinates of the oxygen atom at the 32*e* sites and atomic displacement parameter (ADP) were refined. The occupancy factors of Mn and Ni at the 16*d* sites were refined with the following constraint: Ni+Mn = 100%. The common ADP for the 8*a* and the 16*d* sites was refined.

For the Layered oxide impurity, the structural model of $LiNiO_2$ (ICSD # 78687) was used with fixed chemical composition of $LiNiO_2$. The ADP of the atoms at the 3*a* and 3*b* sites was equated to the common ADP for the 8*a* and the 16*d* sites in the LNMO spinel phase. The ADP of the oxygen atom at the 6*b* sites was equated to the ADP of the oxygen atom at the 32*e* sites in the LNMO spinel phase.

For the Rock salt impurity, the structural model of $Ni_6MnO_8$ (ICSD # 80301) was used. The ADP of the atoms at the 4*a* and the 24*d* sites was equated to the common ADP for the 8*a* and the 16*d* sites in the LNMO spinel phase. The ADP of the oxygen atoms at the 8*c* and 24*e* sites was equated to the oxygen atom at the 32*e* sites in the LNMO spinel phase.

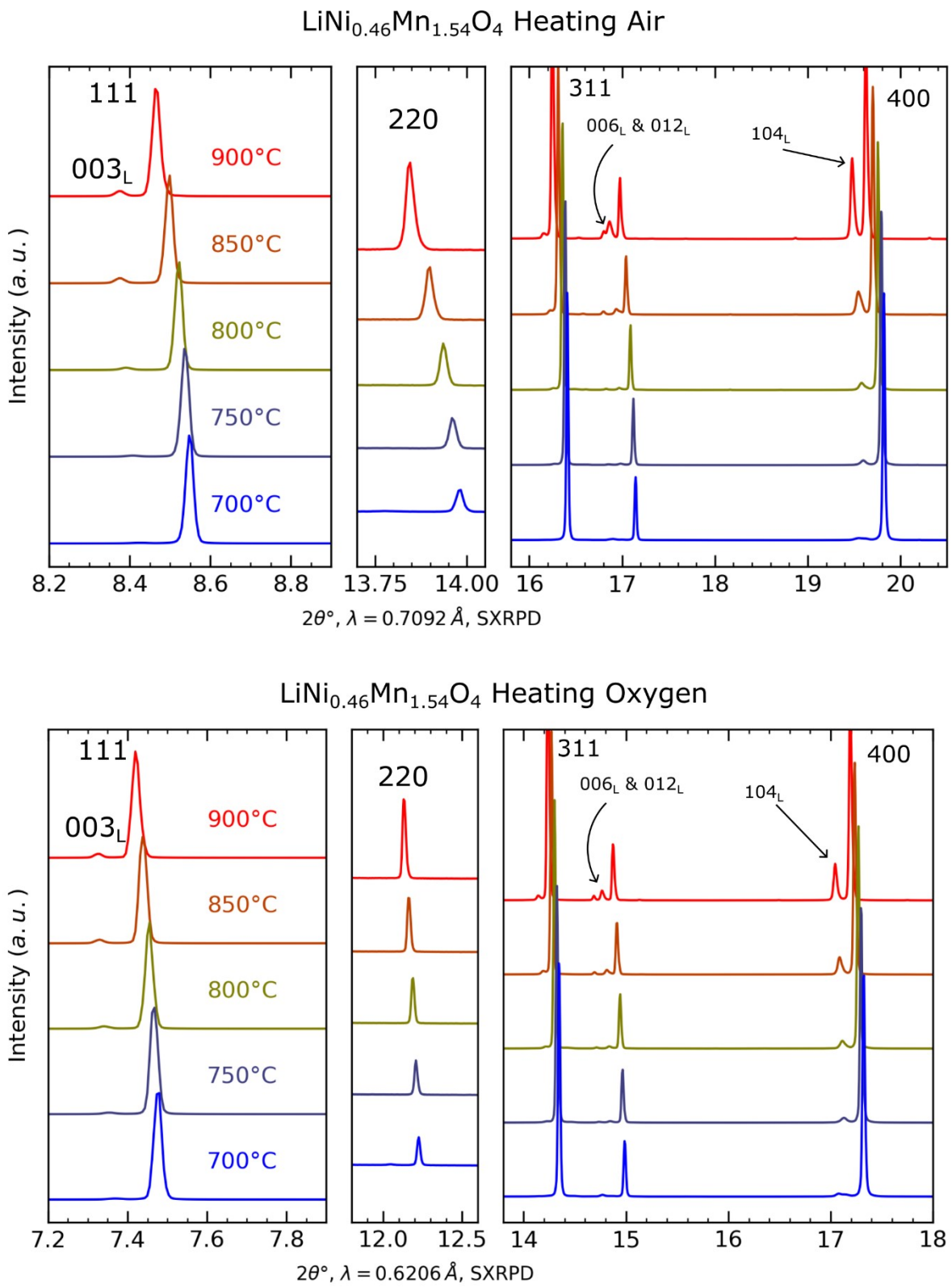


**Figure S5**. Selected 2θ ranges of the *in situ* SXRPD patterns collected upon heating of the pristine LNMO sample at given temperatures, under air (top) and oxygen (bottom) atmospheres.

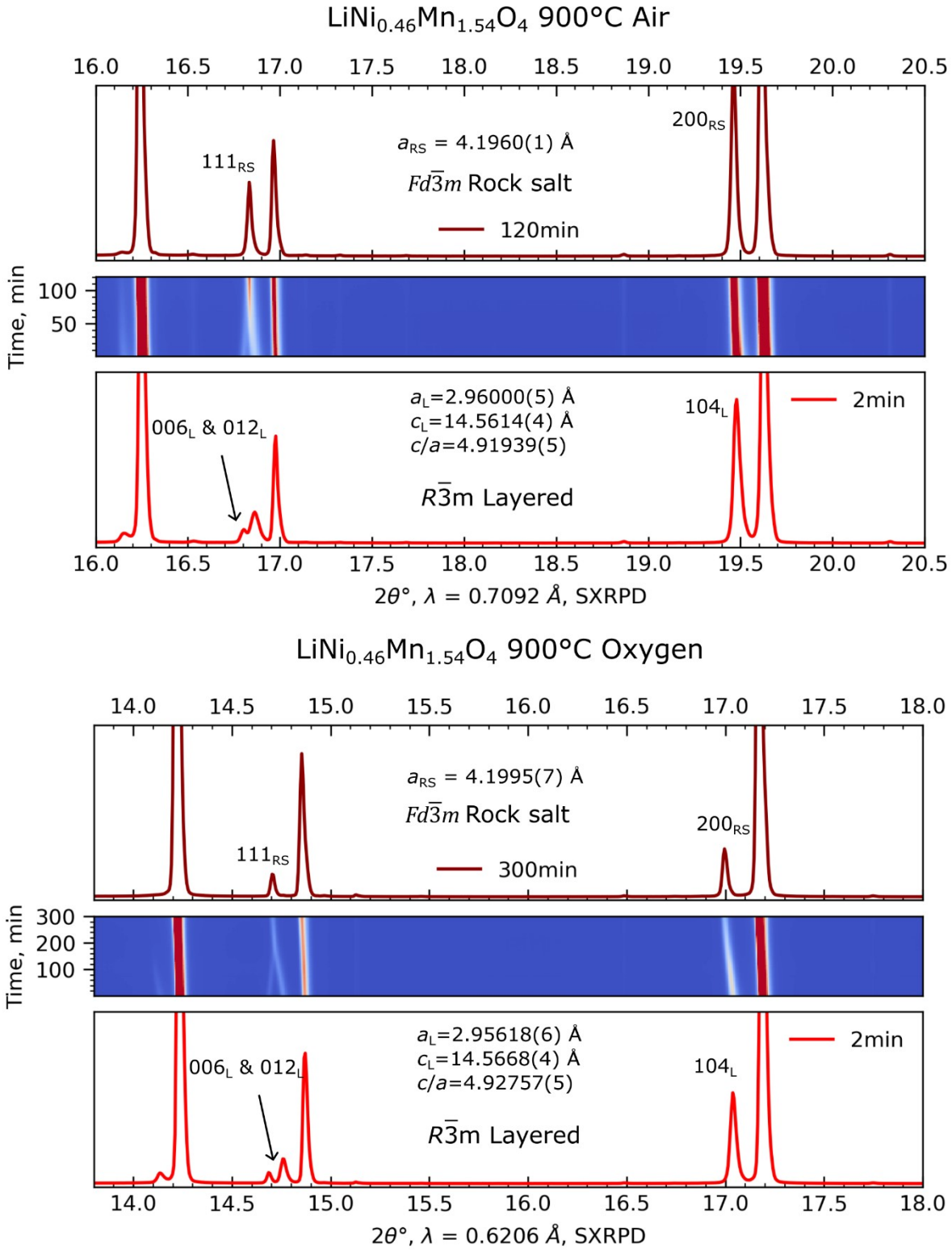


**Figure S6**. Contour plot representing evolution in time of the selected 2θ range of the SXRPD patterns, collected at 900°C under air (top) and oxygen during the *in situ* experiment.

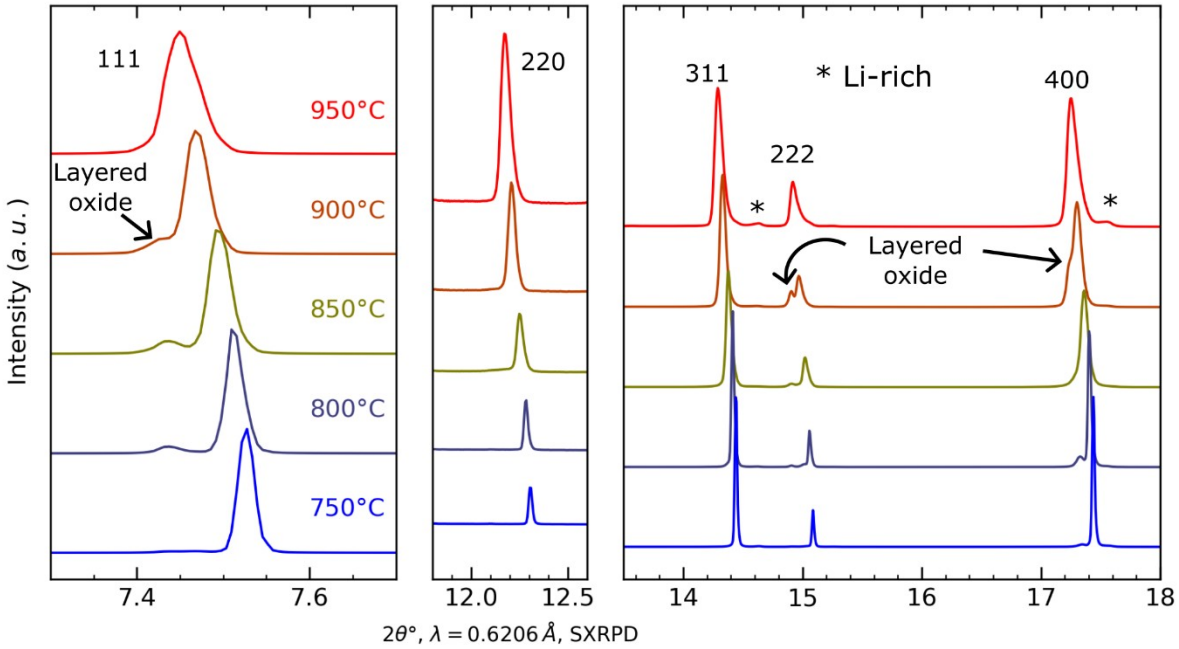


**Figure S7**. Selected 2θ ranges of the SXRPD patterns of the LNMO samples quenched from 750-950°C range.

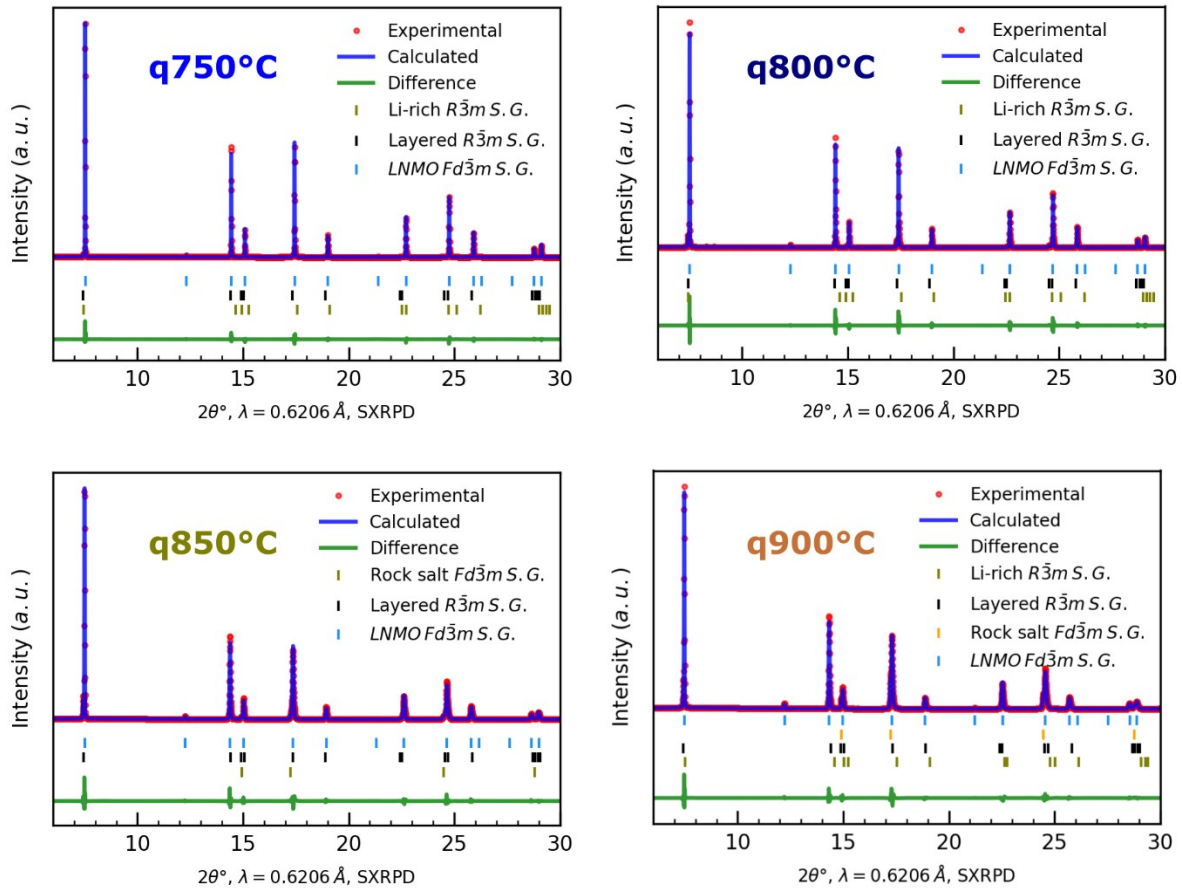


**Figure S8**. Experimental points, calculated and difference plots with corresponding Bragg positions obtained after the Rietveld refinement of SXRPD patterns of the quenched LNMO samples, presented in **Figure S7**.

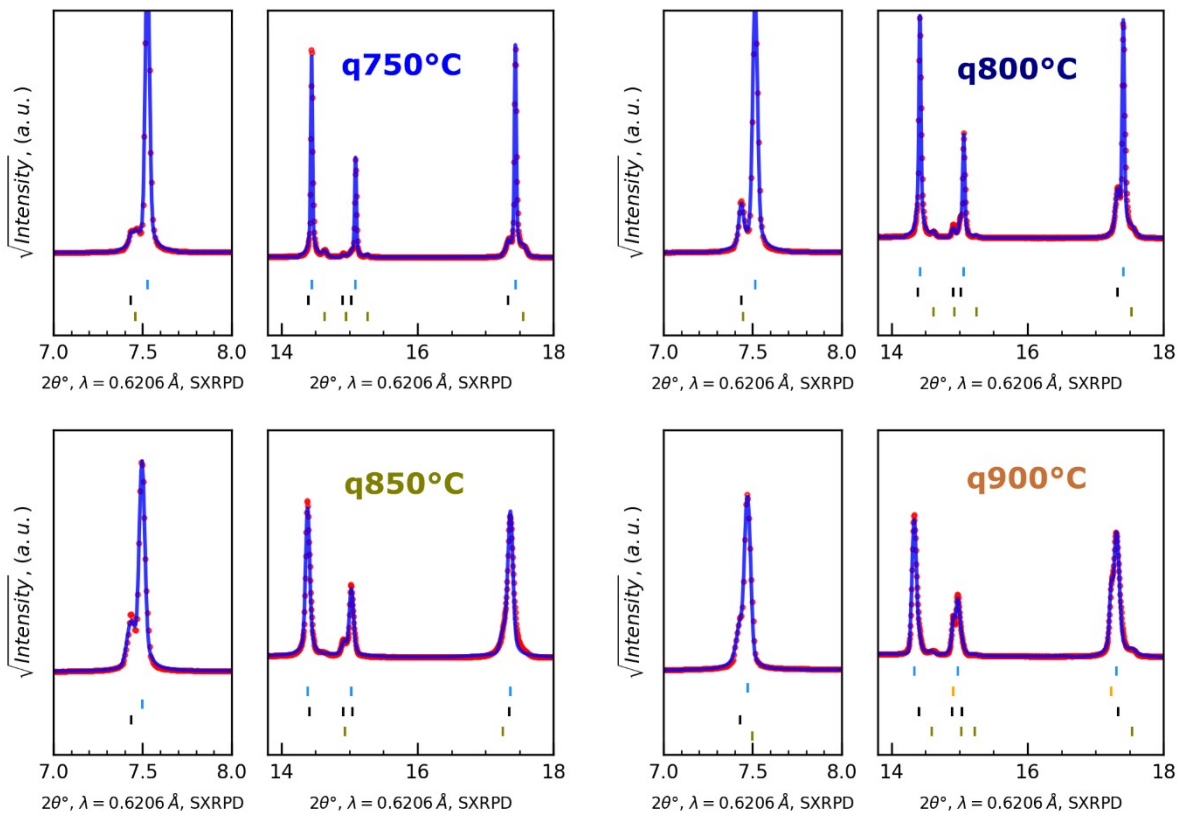


**Figure S9**. Selected 2θ° range of the plots given in **Figure S8**, to illustrate the quality of analysis of impurity phases. The square root scale of intensities was chosen for better illustration of the impurity reflections.

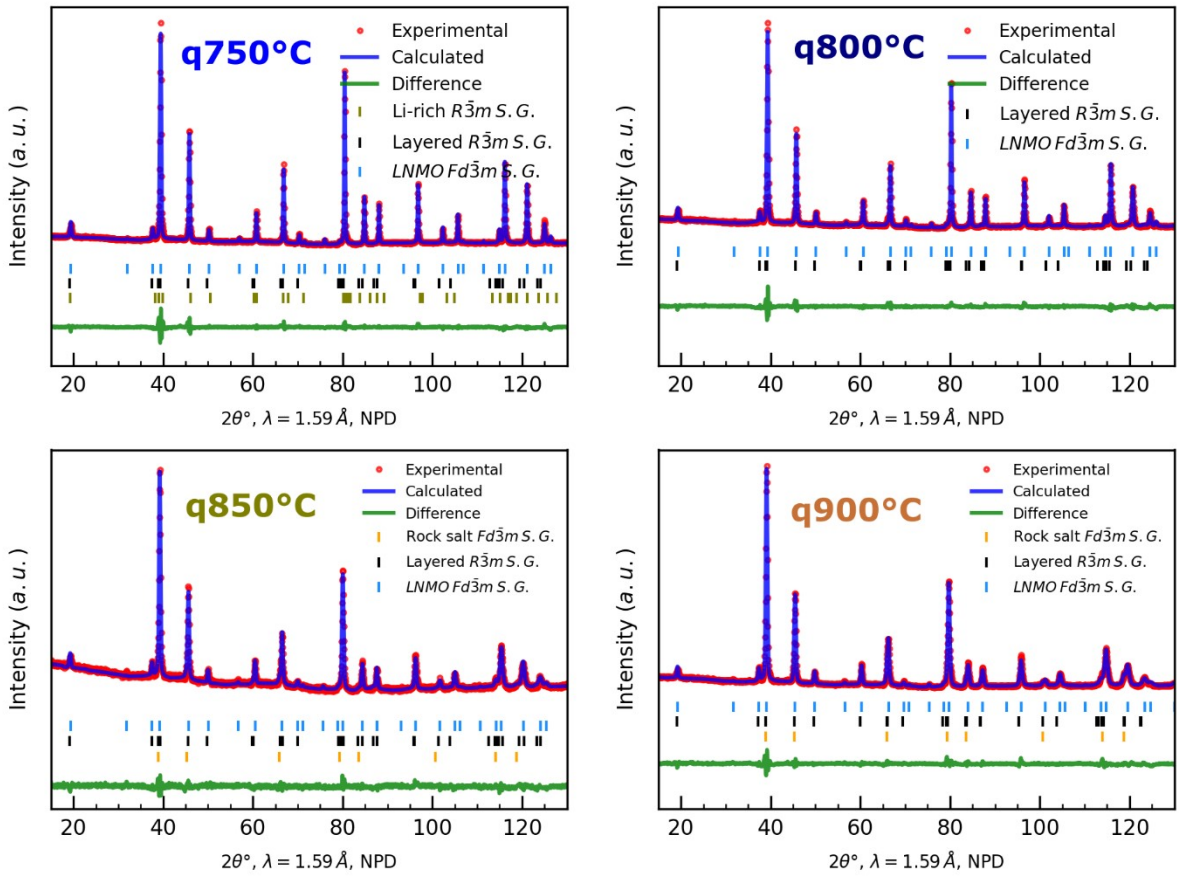


**Figure S10**. Experimental points, calculated and difference plots with corresponding Bragg positions obtained after the Rietveld refinement of NPD patterns of the quenched LNMO samples.

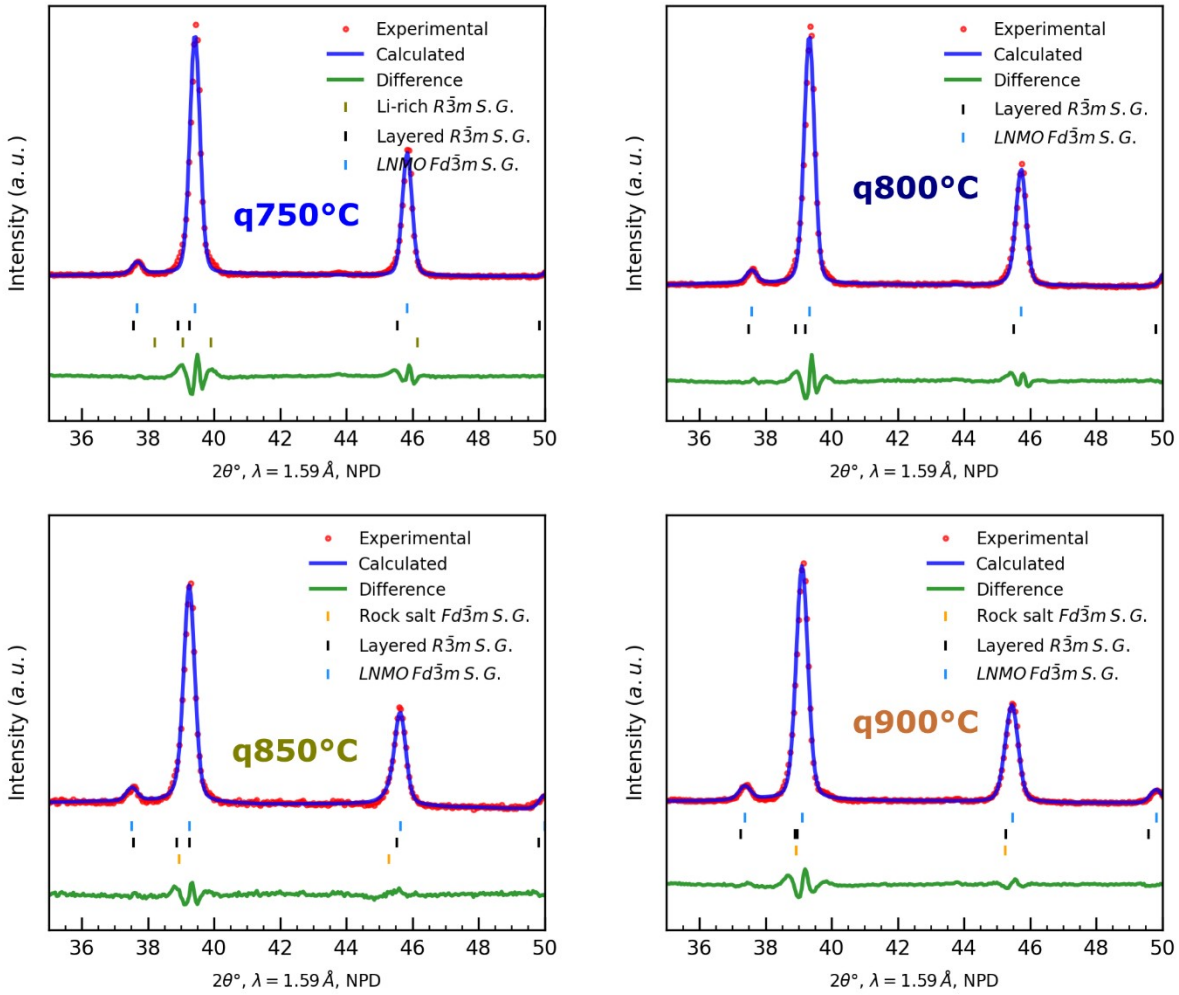


**Figure S11**. Selected 2θ° range of the plots given in **Figure S10**, to illustrate the quality of analysis of impurity phases.

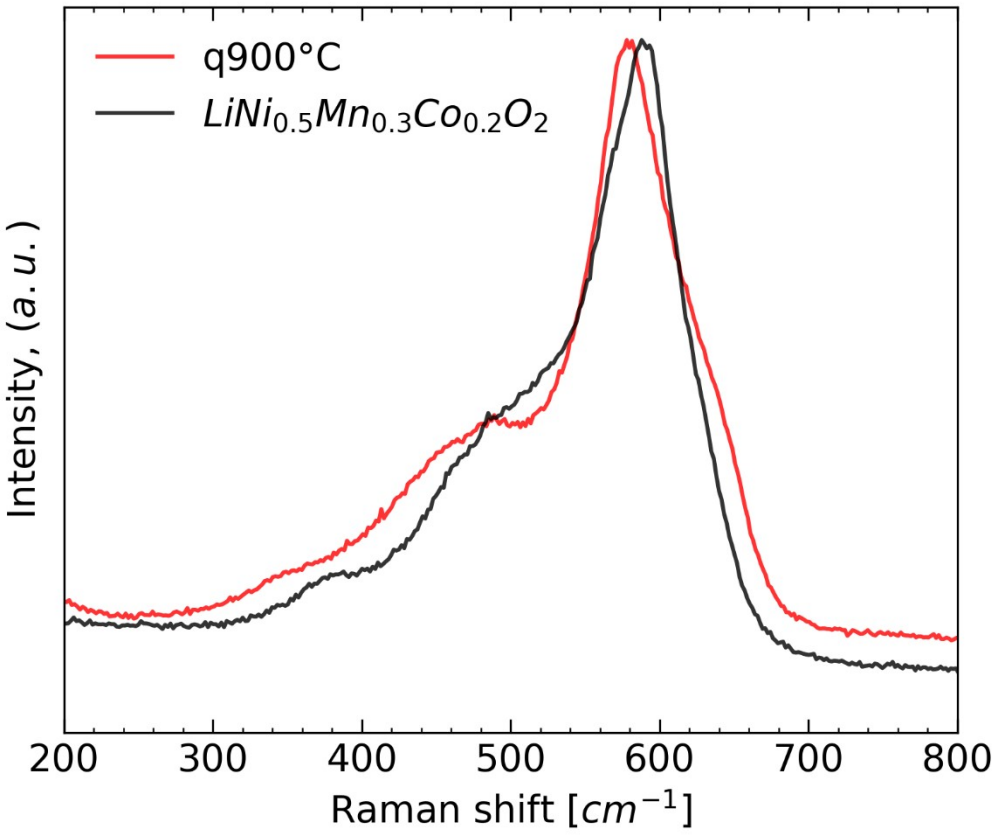


**Figure S12**. Selected Raman spectra of the q900°C sample and the $LiNi_{0.5}Mn_{0.3}Co_{0.2}O_2$.

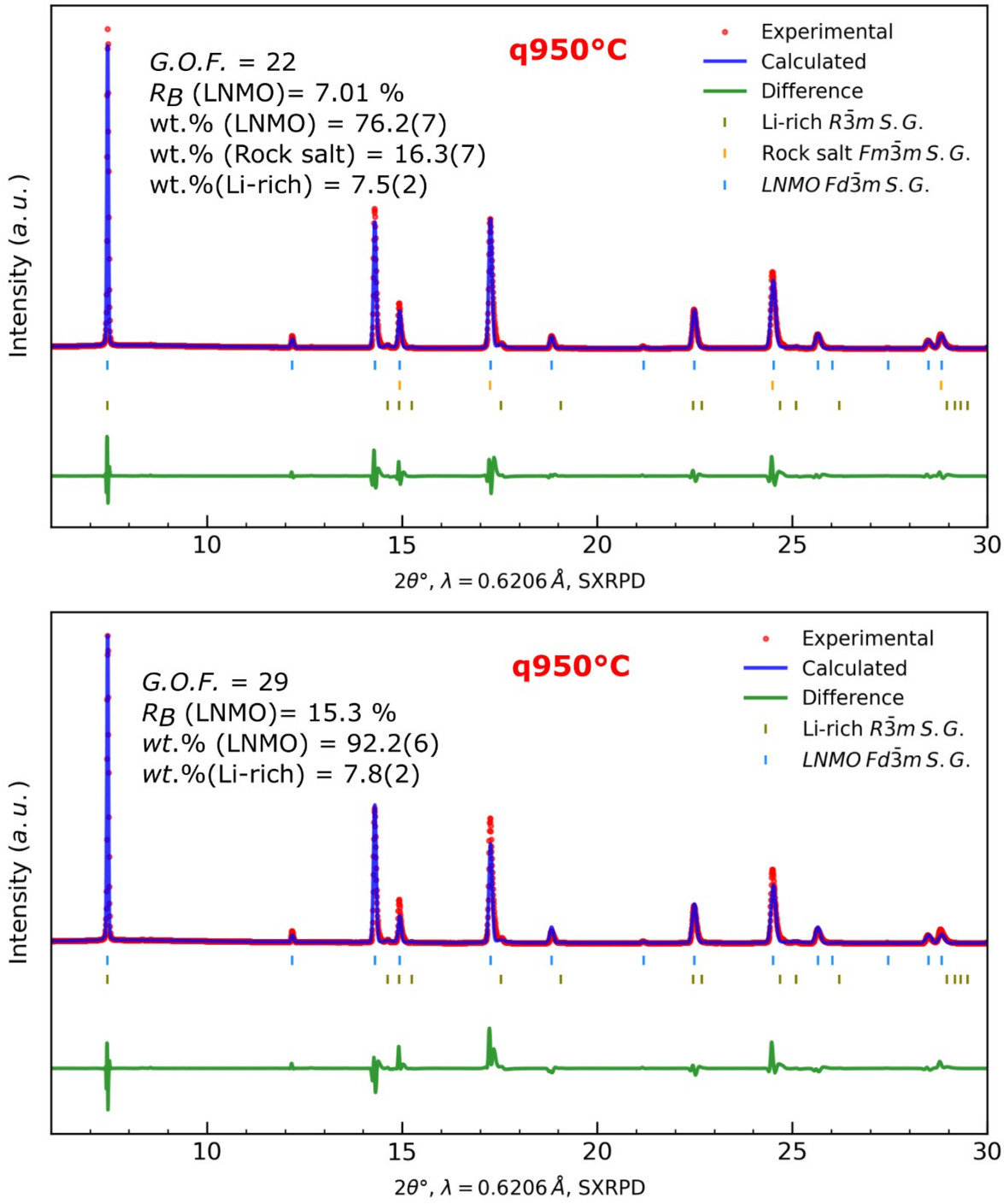


**Figure S13**. Experimental points, as well as calculated and difference profiles after the Rietveld refinement of the SXRPD pattern of the q950°C sample, using three- (left) and two-phase models (right).